

Journal Pre-proof

FT-NIR models for predicting film quality parameters in titanium dioxide-free tablet coatings

Filip Gorachinov , Monika Koviloska , Katerina Tnokovska ,
Ana Atanasova , Packa Antovksa , Jelena Lazova ,
Nikola Geskovski

PII: S0928-0987(24)00305-1
DOI: <https://doi.org/10.1016/j.ejps.2024.106992>
Reference: PHASCI 106992



To appear in: *European Journal of Pharmaceutical Sciences*

Received date: 2 June 2024
Revised date: 30 November 2024
Accepted date: 15 December 2024

Please cite this article as: Filip Gorachinov , Monika Koviloska , Katerina Tnokovska , Ana Atanasova , Packa Antovksa , Jelena Lazova , Nikola Geskovski , FT-NIR models for predicting film quality parameters in titanium dioxide-free tablet coatings, *European Journal of Pharmaceutical Sciences* (2024), doi: <https://doi.org/10.1016/j.ejps.2024.106992>

This is a PDF file of an article that has undergone enhancements after acceptance, such as the addition of a cover page and metadata, and formatting for readability, but it is not yet the definitive version of record. This version will undergo additional copyediting, typesetting and review before it is published in its final form, but we are providing this version to give early visibility of the article. Please note that, during the production process, errors may be discovered which could affect the content, and all legal disclaimers that apply to the journal pertain.

© 2024 Published by Elsevier B.V.
This is an open access article under the CC BY-NC-ND license
(<http://creativecommons.org/licenses/by-nc-nd/4.0/>)

Highlights

- TiO₂-free film coating optimization is challenging in the pharmaceutical industry
- NIR offers a precise and exact method for film coating thickness determination
- MVA methods allow a knowledge-based approach to determine film chemical signals
- Both film thickness and a^* can be used as calibration techniques with high accuracy

Journal Pre-proof

FT-NIR models for predicting film quality parameters in titanium dioxide-free tablet coatings

Filip Gorachinov^{1,2*}, Monika Koviloska¹, Katerina Tnokovska¹, Ana Atanasova¹, Packa Antovksa¹, Jelena Lazova¹, Nikola Geskovski^{2*}

¹Research & Development, Alkaloid AD-Skopje, Blvd. Aleksandar Makedonski 12, 1000, Skopje, N. Macedonia

²Ss. Cyril and Methodius University in Skopje, Faculty of Pharmacy, Institute of Pharmaceutical Technology, Mother Theresa 47, 1000 Skopje, N. Macedonia

Corresponding authors:

Filip Gorachinov
Research & Development, Alkaloid AD-Skopje, Blvd. Aleksandar Makedonski 12, 1000, Skopje, N. Macedonia
Ss. Cyril and Methodius University in Skopje, Faculty of Pharmacy, Institute of Pharmaceutical Technology, Mother Theresa 47, 1000 Skopje, N. Macedonia
e-mail: fgorachinov@alkaloid.com.mk

Nikola Geskovski
Ss. Cyril and Methodius University in Skopje, Faculty of Pharmacy, Institute of Pharmaceutical Technology, Mother Theresa 47, 1000 Skopje, N. Macedonia
e-mail: ngeskovski@ff.ukim.edu.mk

ABSTRACT

This study leverages Fourier Transform Near-Infrared (FT-NIR) spectroscopy to monitor the coating process of pharmaceutical tablets using PVA-based TiO₂-free films, with talc and iron oxides as opacifiers. By employing a combination of multivariate analytical techniques to evaluate the correlation between film coating progression and film thickness. Assessment of coating thickness for different coating levels was performed by optical microscopy. Additionally, using colorimetric analysis by scanner method, the color progression for different coating levels was evaluated and expressed as the a* value from CIELAB color space. The coordinate value a* showed predictable changes with the progression of the coating process and film thickness values, indicating its utility as a robust reference method for quality control and process optimization. The predictive capability of the OPLS models, validated against measured film thickness and the a* value, demonstrated low prediction errors and confirmed the models' effectiveness in distinguishing coating levels and accurately predicting film coating progression. The OPLS model used knowledge-based peaks of interest, which were further confirmed by loading and coefficient plots. The study demonstrated that film thickness, as a destructive, and a* value from CIELAB color space, as a non-destructive reference method for coating progression could be used during a controlled pharmaceutical coating process for product quality assessment and pharmaceutical process endpoint determination.

Keywords: FT-NIR, Process analytical technology, Film thickness, Titanium dioxide-free film coating, Multivariate analysis

1. Introduction

In pharmaceutical manufacturing, coatings are widely employed to enhance organoleptic properties, improve the physical and chemical stability of solid dosage forms, and potentially modify dissolution profiles (Zaid, 2020). Even with immediate-release coatings, the impact on dissolution becomes more pronounced as the thickness increases. Thicker coatings reduce liquid ingress initially, affecting the overall dissolution rate, a critical quality attribute (CQA) for these dosage forms. This highlights the necessity of developing process analytical technology (PAT) tools that would enable accurate coating process and product control (Dong et al., 2023). A tablet coating process should result in a constant thickness of the coating layer and uniform and visually identical coating of all tablets. To ensure the quality and safety of different pharmaceutical products, the European Medicines Agency (EMA) has issued several guides on real-time testing and requirements for using various spectroscopic techniques during new submissions and variations (European Medicines Agency, 2014). Titanium dioxide (TiO₂) is currently widely used as an opacifier in tablet film coatings to enhance the appearance and stability of pharmaceutical products and is effective in relatively thin films and at low concentrations. Recently, the European Food Safety Authority (EFSA) modified its stance on titanium dioxide, previously deemed safe as a food additive, by questioning its safety based on new studies and the particles' potential to accumulate in the body despite their low absorption rate. Commission Regulation (EU) 2022/63 bans the use of TiO₂ in food and urges the pharmaceutical industry to expedite research and development efforts to replace titanium dioxide in both new and existing products (Blundell et al., 2022). The multifunctional attributes of TiO₂ make it challenging

to replace with one or a combination of excipients like calcium carbonate (CaCO_3), talc, iron oxides, zinc oxide (ZnO), calcium carbonate/calcium hydrogen phosphate ($\text{CaCO}_3/\text{CaHPO}_4$) (Radtke et al., 2021). Titanium dioxide-free films, which exhibit lower opacity, lower contrast ratio, and reduced capability to protect from photodegradation and moisture, typically require a weight gain of 5 to 8% and a thicker film to match the performance of TiO_2 . This could potentially lead to increased dissolution time and a need for more precise film coating process monitoring and quality control (Gallo et al., 2023; Palugan et al., 2022).

Several parameters are used to monitor the film coating process and assess the quality of the film coating, with a primary focus on coating thickness and the amount of polymer applied to tablet cores (Gendre et al., 2011). Noninvasive and simple reference measurements, such as conventional weight gain measurements, correlate poorly with film coating thickness and require the averaging of a large number of tablets to overcome inaccuracies due to weight variation (Alves-Lima et al., 2020; Möltgen et al., 2012; Römer et al., 2008; Wahl et al., 2019). Optical microscopy, while expected to yield better results as a calibration reference method, also has limitations: film-thickness measurements are invasive, time-consuming, and susceptible to operator error and personal bias. These issues arise from core-film interactions and the absence of perfectly linear core/coating interfaces. To mitigate these challenges, measurements are often taken by multiple independent analysts (Römer et al., 2008; Wahl et al., 2019). In addition, the coating layer exhibits inherent thickness variability due to unavoidable inter- and intra-tablet coating inconsistencies. This variability is reflected in film coating thickness measurements regardless of the method used and should not be mistaken for measurement error (Wahl et al., 2019). To improve the objectivity of film coating process analyses, more advanced instrumental methods with high repeatability are used. These include optical coherence tomography (OCT) for films from 10-60 μm (Li et al., 2014; Markl et al., 2015), dynamic image analysis (Czajkowska et al., 2015), terahertz pulse imaging (TPI) for films of 40 μm and thicker (Brock et al., 2012; Haaser et al., 2013), and FT-NIR diffuse reflectance spectroscopy (Hattori et al., 2018). Optical microscopy, a well-established method for measuring film thickness through direct visual inspection, is often used as a reference to validate advanced techniques like FT-NIR, OCT, and TPI, given its strong correlation with these methods (Farkas et al., 2021; Wolfgang et al., 2019). In addition to optical microscopy, various image analysis techniques are explored for quality control in evaluating film coating thickness and the overall coating process. An interesting application of image analysis, in combination with neural networks (YOLOv5) discussed by Ficzer et al. (2022), also plays a valuable role in the prediction of film thickness through tablet diameter variation and classification of tablet defects (Ficzer et al., 2022). Color image analysis is increasingly being utilized as a method for studying film thickness and assessing the film coating process in colored film-coated tablets (Farkas et al., 2021). Murillo et al. demonstrated that color and appearance are expected to change predictably and exponentially with the progression of the film coating process and eventually stabilize asymptotically with further changes in the concentration of film components (Murillo et al., 2018). Therefore, some CIELAB parameters and hue can be used to track color evolution, coating quality, and film thickness in a non-invasive manner (Murillo et al., 2018; Turk et al., 2021). Chemical components that cause color variations can absorb light in the NIR region, allowing for a correlation between color evolution and NIR spectroscopy. Consequently, methods like NIR could provide a comprehensive and reliable assessment of coating progression in pharmaceutical applications. Although values like hue and CIELAB parameters have been used to predict film thickness and track the evolution of pharmaceutical film coating (Murillo et al., 2018; Turk et al., 2021), there are no literature data regarding the correlation of NIR spectral information

with CIELAB parameters as a non-invasive reference technique for the tracking of film coating progression with TiO₂-free film coatings.

Therefore, the aim of our work was to evaluate the possibility of utilizing Fourier Transform Near-Infrared (FT-NIR) spectroscopy to monitor the coating process of pharmaceutical tablets using TiO₂-free films (proprietary PVA-based TiO₂-free film coating formula with talc and iron oxides as opacifiers). Film coating thickness for different coating levels was assessed using optical microscopy. Additionally, scanner-based colorimetric analysis was employed to monitor the color progression of different coating levels using CIELAB color space parameters. Unsupervised and supervised multivariate models were applied to analyze and correlate NIR spectral variations with film thickness progression and color evolution.

2. Materials and Methods

2.1. Materials

Core composition: Cellulose, Microcrystalline (Avicel PH 102, Du Pont, USA), Dibasic Calcium Phosphate anhydrous (Di-CAFOS A 60 Budenheim; Germany), Copovidone (Kollidon VA 64 BASF, Germany), Croscarmellose sodium (Ac-Di-Sol; Du Pont), Silica, Colloidal anhydrous (Aerosil 200; Evonik, Germany), Magnesium Stearate (FACI S.p.A. -Carascp GE -Italy).

Film coating system: PVA-based TiO₂-free film coating (Opadry TF®; proprietary formula containing partially hydrolyzed Polyvinyl alcohol (PVA), talc, PEG 3350, and iron oxides yellow, red; Colorcon Inc, UK)

2.2. Preparation of tablet cores

A premixture of Silica, Colloidal anhydrous (1.25%) was prepared with Cellulose, Microcrystalline (3.75%) in an Aeromatic Fielder PMA 300 (GEA, Germany) high shear mixer (1 minute at 150 rpm impeller speed). Mixture for tablet placebo cores was prepared by dry mixing of premixture with the rest of Cellulose, Microcrystalline (60.00%), Dibasic Calcium Phosphate anhydrous (30.00%), Copovidone (1.00%), Croscarmellose sodium (2.00%) in Aeromatic Fielder PMA 300 high shear mixer for 4 minutes at 150 rpm impeller speed. After 4 minutes of mixing, 2.00% of Magnesium stearate was added and mixed for 2 minutes at 130 rpm impeller speed. All excipients were sieved through a Russel sieve (1 mm; Russel Finnex N.V., Belgium) prior to mixing. After mixing, the placebo blend was tableted using a Fette 2090 i (Fette Compacting GmbH, Germany) industrial-size tableting machine. The following conditions were used for the preparation of biconvex tablet cores with a diameter of 8 mm and a mass of 200 mg ± 5.0%: pre-compression force 1.2 kN, compression force 16.5 kN, tableting speed 70 000 tbl/h.

2.3. Coating process and sampling procedure

Tablets were coated with an aqueous partially hydrolyzed PVA film coating (PVA-based TiO₂-free film coating) in an industrial-size partially perforated pan coater (Glatt GMPC, x2; Glatt GmbH, Binzen, Germany). The pan load was 21 kg. Spray gun parameters were: spray nozzle diameter 1.2 mm; atomizing air pressure was 2.0 bar; pattern air pressure was 2.2 bar. Samples were collected at coating levels corresponding to 3.6 L, 4.0 L, 4.3 L, and 4.7 L of coating suspension spent (solids 24.57%). The final coating achieved 5.5% tablet weight gain.

Table 1. Parameters of the film coating process

Parameter	Pre-heating	Spraying	Drying	Cooling
Inlet air (m ³ /h)	700	700	700	700
Inlet air temperature (°C)	70	70	70	30
Outlet air temperature (°C)	45-48	45-48	40	30
ΔP drum (Pa)	-150	-150	-150	-150
Drum speed (rpm)	2,3 (10s/60s; Jog)	16	2,3 (10s/60s; Jog)	2,3 (10s/60s; Jog)
Spray rate (ml/min)		50		
Drying time (min)			5	

2.4. NIR measurements and multivariate analysis

240 individual tablets were recorded using an Antaris II FT-NIR analyzer (4000 cm⁻¹ to 10 000 cm⁻¹; 4 nm resolution; OMNIC; Thermo Fisher Scientific, US; SabIR fiber optic diffuse reflectance probe) and used as a calibration set. Spectra were taken in a well-controlled environment (temperature and moisture). A background scan was taken before each recording to minimize instrument drift, and the NIR probe was carefully positioned. Spectra that perform differently than the group, deviating or aberrant spectra whose outlying position cannot be explained as a mere shift along the general trend or orientation of the data, were removed by visual inspection during recording and re-recorded.

Spectra visualization was performed using Spectragryph 1.2. Multivariate analysis was performed in SIMCA 14.1. Models were externally validated by recording a separate batch of 80 tablets. R²X is the cumulative explained variance of the X-matrix (independent variables) by the models. R²X was used as one of the indicators to estimate the models' ability to capture variation in the X data.

$$R_X^2 = 1 - \frac{\sum(x_i - \hat{x}_i)^2}{\sum(x_i - \hat{x})^2}$$

- x_i : The actual value of the variable i in the original dataset
- \hat{x}_i : The predicted value of x_i
- \hat{x} : The mean of the variable x_i
- $\sum(x_i - \hat{x}_i)^2$: The residual sum of squares
- $\sum(x_i - \hat{x})^2$: The total sum of squares

RMSEE (root mean square error of estimation) measures the difference between the observed and predicted values during the training phase, with lower RMSEE indicating better model performance on the training data.

$$\text{RMSEE} = \sqrt{\frac{1}{n} \sum_{i=1}^n (y_i - \hat{y}_i)^2}$$

- y_i : Actual observed value.
- \hat{y}_i : Predicted value by the model.

- n : Number of observations.

RMSEcv (root mean square error of cross-validation) is the RMSEE calculated during cross-validation. Cross-validation was performed using the leave-one-out (LOOcv) method, which is particularly advantageous for moderate-sized datasets (Chen and White, 2024). The selection of LOOcv was based on its ability to provide consistent error estimates across different validation approaches and data sizes, making it suitable for ongoing model development. An external dataset was used to mitigate the possibility of over-optimism. RMSEP (root mean square error of prediction) explains the difference between the observed and predicted values using an independent test set. RMSEP was used to indicate the generalizability and validity of the model's training and cross-validation values.

2.5. Reference measurements

2.5.1. CIELAB color space measurements

The CIELAB color space and its Cartesian coordinate a^* were used for NIR model calibration. The method for tablet scanning was done according to Turk et al. (2021), who used a photo scanner to scan mini tablets and found a correlation between the hue value and coating thickness (Turk et al., 2021). After tablet sampling, measurements were taken for analysis at four coating levels, namely 3.6 L, 4.0 L, 4.3 L, and 4.7 L. A scanner, Canon CanoScan 9000F Mark II (48-bit internal color depth for accurate color rendition with turned-off color correction settings), was used at 600 dpi to capture the variability in color between batches, and it proved sufficient to detect the trend increase in coating thickness between tablet coating levels, considering the uniform light source across the sample, high color gamut as well as the fixed angle and position under which the tablets were recorded. Tablets were placed consistently in the same position on the scanner bed. CIELAB parameters were extracted using Fiji/ImageJ (Schindelin et al., 2012) and were used for color analysis. The RGB parameters were converted to CIELAB using Fiji/ImageJ, and an a^* value was extracted. The calculated ΔE value between the highest and lowest coating levels, with the lowest color level as the reference, indicates that the system accurately detected subtle color variations. ΔE value of 9 was found, signifying that the system successfully captured perceptible differences between the color levels. Furthermore, the scans were all performed in quick succession, avoiding potential inaccuracies due to changes in environmental conditions or equipment wear. The evolution of color (Figure 1) matched previously reported color parameters for coated tablets (Murillo et al., 2018).

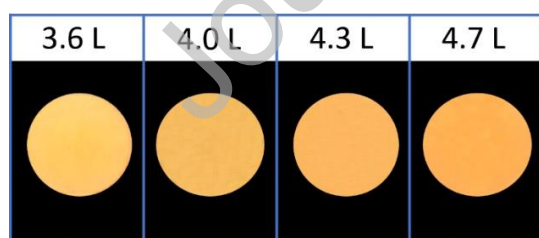


Figure 1. Change of color of randomly selected tablets with coating at various levels of expended film coating suspension

2.5.2. Film thickness measurements

The film-coated tablets were cut using the blade of a tablet cutter (fine blade microtome). Film thickness was measured using optical microscopy (Stemi 305; Zeiss, Germany; Zeiss Zen 3.8 software; 5x

magnification), ensuring a consistent angle. The thickness was measured at five points near the apex of the tablet and averaged, ensuring consistent readings. Despite labor intensiveness, this method proved accurate for our analyses. All the tablets from different coating levels recorded by NIR (240 tablets in the calibration set and 80 tablets in the test set) were measured separately for film thickness, as displayed in Figure 2, to ensure the model's maximal accuracy.

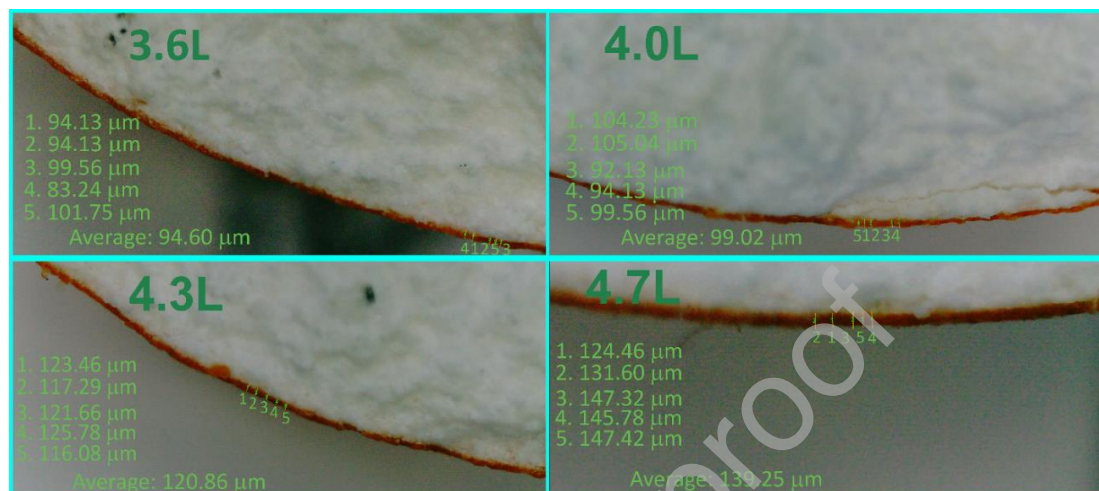


Figure 2. Change of film thickness of randomly selected tablets with coating at various levels of expended film coating suspension

2.5.3. LOD measurements

Loss-on-drying (LOD) was measured using Mettler LP16 moisture analyzer (Mettler-Tolledo, Zaventem, Belgium) on a 2g sample at a temperature of 105 °C until mass remained constant for 5 minutes.

3. Results and Discussion

3.1. Reference methods

Two reference methods were used: optical microscopy as a destructive method to measure film thickness, and a^* from the CIELAB color space as a nondestructive indicator of coating progression. The values of film thickness growth and a^* across different coating levels (3.6L-4.7L) are presented in the dual-axis plot (Figure 3). Considering the nature of the spray coating process, inter-tablet variability of the film thickness for each coating level is expected. The dual-axis plot illustrates the distribution of film thickness values across randomly sampled tablets at various coating levels, reflecting inherent inter-tablet variability typical of the pan-coating process. The upward trend for four distinct coating levels shows the progression of coating. In this study, the pan-coating process demonstrates increasing inter-tablet uniformity with time (Figure S1a), and low inter-tablet covariance (Figure S1b; 80 tablets per coating level), which remains low and decreases further as coating levels increase, validating the process's effective design (Mostafaei et al., 2023; Zhang et al., 2017). From the CIELAB parameters, the average of L^* decreased with the progression of film coating, the average of b^* remained nearly constant, and the average of a^* increased with the progression of film coating. During our preliminary studies and sample evaluation for the development of the current model, it was found that there was an expected trend of growth between a^* (CIELAB value) and the progression of the film coating process, indicating its usefulness as a simple method

for calibration (Figure 3). Murillo et al. explored color evolution during the pan coating and used CIELAB values to monitor coating uniformity and variability to advance toward automated control of the coating process. They noticed an increase in a^* values throughout the coating process, indicating accumulation of the coating material. The progression towards higher a^* values is consistent with the expected outcome of coating the tablets with a colorant that includes components contributing to redness (Murillo et al., 2018). In our case, the usefulness is justified by the fact that the film coating progress generates an increase in the intensity of chemical signals from PVA-based TiO_2 -free film, an increase in coating thickness, and an increase in pigments, opacifiers, and other components of the film. These factors directly affect the color of the tablets, and consequently result in a positive change in a^* from the CIELAB system. Color perception in thick films varies with thickness due to absorption differences, which depends on the material's chemical composition, light path length, and scattering. In thicker films with heterogeneous compositions, light scattering can alter the intensity and distribution of light exiting the film, thus changing its appearance. The bending of light or refraction can also play a significant role in the color perception of thicker films. Namely, film thickness can alter the path of light through a material, affecting the perceived color, while the amount of light reflected versus absorbed depends upon multiple internal reflections, which can compound and affect the color (Mortimer et al., 2009). In summary, the perception of color depends on the molecular composition of the film and the physical structure, namely surface roughness, and film uniformity, as they can all impact how light interacts with the film. Although we are building the model based on a small range of film coating levels, we can observe the difference in appearance due to changes in film thickness. These differences were quantified using CIELAB values (Figure 3).

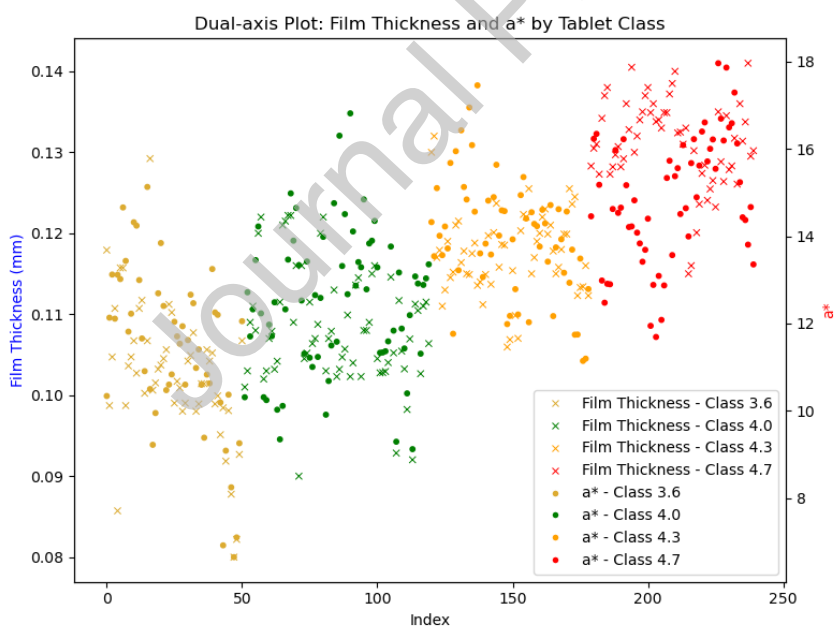


Figure 3. Dual-axis plot of film thickness and a^* values

3.2. Spectroscopic interpretation of the signals of interest

The spectra of the film-coated tablets consist of signals from multiple variables arising due to chemical and physical changes during the coating process. Pharmaceutical film coatings are heterogeneous mixtures of chemical compounds. They produce a combined spectral response to incident light in the NIR spectral region, which is defined by multiple physical and chemical characteristics. Consequently, the reflectance spectra are not always linear combinations of signals from individual film components (Römer et al., 2008). The transmittance of the coating material may cause variations in reflectance measurements influenced by multiple scattering events from differences in particle size, shape, film microstructure, roughness, thickness, opacity, and morphology, and illumination geometry, which generate spectral changes unrelated to the chemical changes during the film growth process. Due to the inherent complexity of NIR spectra as well as the heterogeneous mixtures being recorded, namely multi-component pharmaceutical film coatings and tablet cores, NIR spectra are often a combination of a broad range of overlapping absorption bands originating from overtones and combination-vibration bands usually found in more complex molecules (Beć et al., 2020; Pomerantsev et al., 2017). The overlapping and broad nature of NIR spectra makes it challenging to assign specific spectral features to target changes without applying chemometric methods such as PCA, which enable the identification of subtle variations related to product qualities (Ciurczak et al., 2021).

To trace back the characteristics of the NIR spectrum to specific attributes of the system's chemistry, we tried to understand and correlate variations in well-defined parts of the spectrum with the measured properties. The spectra of film-coated tablets closely resemble those of the PVA-based, TiO₂-free film coating. Therefore, we first evaluated the spectra for any meaningful contribution of the PVA-based TiO₂-free film coating components, which may enable the development of a robust prediction model.

One narrow, very prominent, and one weak peak of PVA-based TiO₂-free film coating was found in the 7000-7250 cm⁻¹ region belonging to the first fundamental overtone of the OH stretching vibration. The absorption peak at 7185 cm⁻¹ is sharp and strong, while the 7152 cm⁻¹ peak is weaker in both the film-coated tablet and PVA-based TiO₂-free coating (Figure 4a; Figure 4c1). Several studies have described both the prominent and weak peaks as characteristic of Opadry® films (Maurer and Leuenberger, 2009). The only constituent of the PVA-based TiO₂-free film coating to exhibit a sharp, very strong, prominent peak at 7185 cm⁻¹ was talc (Figure 4a) (Petit et al., 2004).

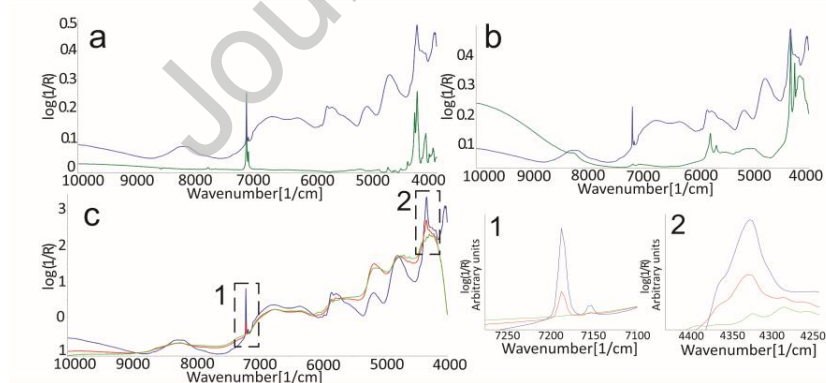


Figure 4. a) Spectra of talc (green) and PVA-based TiO₂-free film coating (blue); b) Spectrum of PVA-based TiO₂-free film coating (blue) and iron oxide yellow (green); c) Overlaid spectra of PVA-based TiO₂-free film coating (blue), the tablet core (green), and film-coated tablet (red), box 1 7185 cm⁻¹ peak region, box 2 4324 cm⁻¹ peak region; 1 -shows that the peak at 7185 cm⁻¹ is present in film-coated tablets and PVA-

based TiO_2 -free film coating but not in the tablet core; 2 - shows the prominence of the peak at 4324 cm^{-1} of the film-coated tablets and PVA-based TiO_2 -free film coating.

The peak of talc at 7185 cm^{-1} has been described as the first overtone ($2\nu\text{Mg}_3\text{OH}$) of vibrations of structural OH groups and is characterized by a position and shape irrespective of concentration. In addition to the $2\nu\text{Mg}_3\text{OH}$ peak at 7185 cm^{-1} , another peak at 7152 cm^{-1} in the PVA-based TiO_2 -free film coating and film-coated tablets, characteristic of talc, can be assigned to $2\nu\text{Mg}_2\text{FeOH}$ (Fe substitution in talc) (Petit et al., 2004; Wu et al., 2022). Further analysis has confirmed that the peak at 7185 cm^{-1} grows as film coating progresses, confirming its utility for tracking the progression of the film coating process (Figure 5).

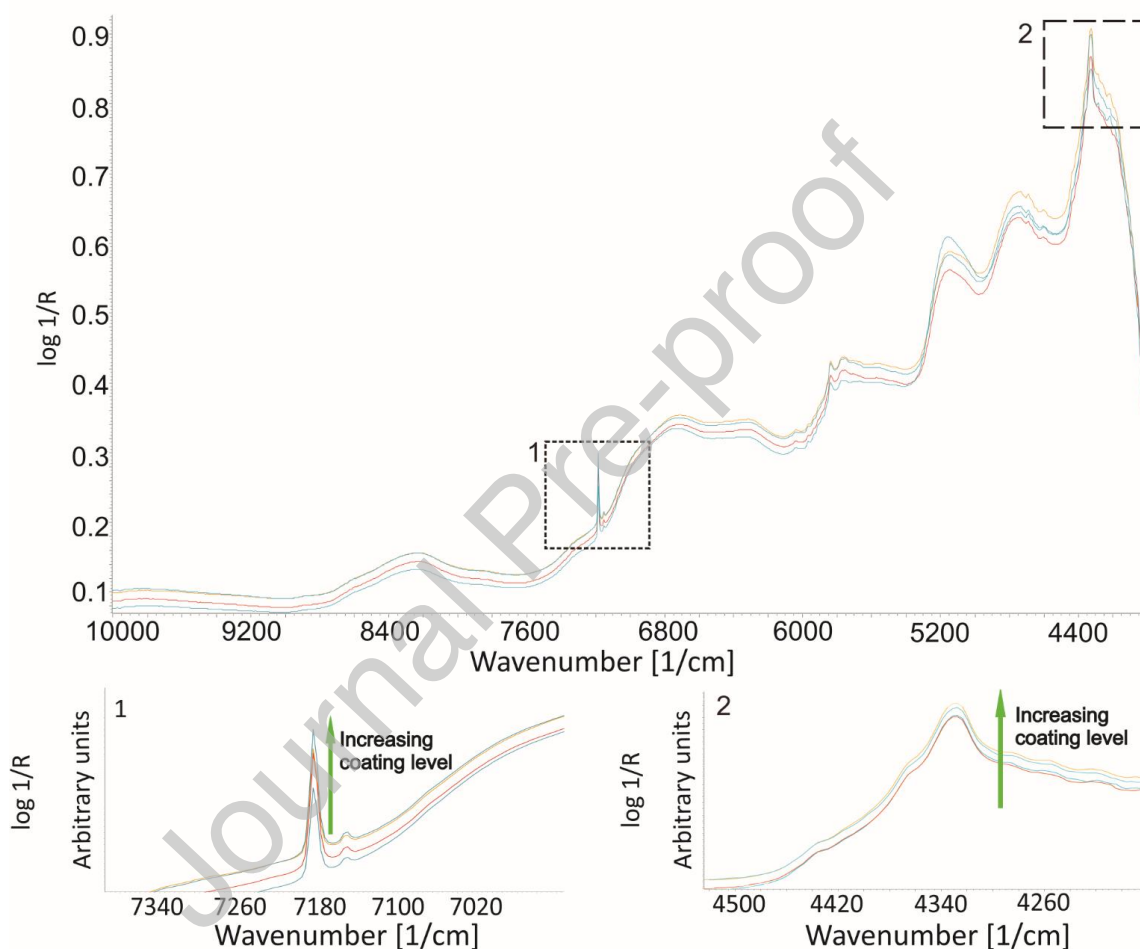


Figure 5. Comparison of spectra from multiple coating levels and most characteristic peaks, which change with coating level; box 1 - the peak at 7185 cm^{-1} ; box 2 - the peak at 4324 cm^{-1} ; 1 - shows the increase along the $\log 1/R$ axis with increasing coating level at 7185 cm^{-1} ; 2 - shows the increase along the $\log 1/R$ axis with increasing coating level at 4324 cm^{-1}

In addition to the peak at 7185 cm^{-1} , another very prominent band specific for PVA-based TiO_2 -free film coating showing increasing intensity on the $\log 1/R$ axis with increasing coating level was found at 4324 cm^{-1} (Fig 4c2). The region from $4400\text{--}4200\text{ cm}^{-1}$ (peak at 4324 cm^{-1}), which intensifies with the progression of film coating, is composed of overlapping absorption bands of different coating components. As

presented in Table 2, talc shows a strong and sharp OH stretching at 4324 cm^{-1} (Wu et al., 2022), PEG 3350 shows CH-stretching and CH-bending combination bands at 4331 cm^{-1} , and PVA displays C-H₂ stretching and =C-H₂ bending combination bands at 4266 cm^{-1} (Conzen, 2014). The spectra of film components that contribute to this band (4324 cm^{-1}), PVA, PEG, and talc, are presented in Figure S3. During inspection of the raw spectra, the overall trend of the peak intensity for coated tablets increases during film coating progression. The only spectral feature showing the opposite trend is the $5290 - 5000\text{ cm}^{-1}$ region (peak at 5141 cm^{-1}), which corresponds to the -OH combination band originating both from the core and coating components and exhibiting an intensity decrease due to changes in water content during the coating process (Möltgen et al., 2012).

In addition, literature data proposes that the absorption band extension at approximately 9000 cm^{-1} into the NIR region beyond $10\,000\text{ cm}^{-1}$ (from $10\,000\text{ cm}^{-1}$ to 9000 cm^{-1}) might be due to a combination of fundamental electronic transitions, overtones, and the physical and crystallographic properties of the pigment E172 (iron oxide red, iron oxide yellow). Reflectance spectra of iron oxides in the near-IR and visible light result from crystal-field transitions of Fe^{3+} in octahedral and tetrahedral coordination. Scheinost and Schwertmann (1997), described a peak of unsubstituted goethite centered at the wavelength of $1\ \mu\text{m}$ (1000 nm ; wavenumber $10\,000\text{ cm}^{-1}$). This change in the log 1/R axis originates from the ${}^4\text{T}_{1g}$ ferric iron transition peak (d-d transition) and is prominent in the spectra of iron oxide E172 compared to the PVA-based TiO_2 -free film coating mixture (Figure 4b is a comparison of PVA based TiO_2 free film coating and iron oxide yellow; the spectra of both, the yellow and red iron oxide pigment are presented in Figure S2) (Scheinost and Schwertmann, 1997). The lower intensity on the log 1/R axis in the PVA-based TiO_2 -free film coating mixture and film-coated tablets compared to the iron oxide pigment in the region $10\,000\text{ cm}^{-1}$ to 8000 cm^{-1} may be attributed to the interactions within the mixture of organic and inorganic components in the PVA-based TiO_2 -free film coating (Ben-Dor, 2002; Morris et al., 1985; Zheng et al., 2019). These interactions result in complex effects on spectral features, likely altering intensity along the log 1/R axis and peak positions of some bands and areas under each peak (Zheng et al., 2019). The significance of this region will be further explored in PCA/OPLS analysis.

In general, the overtones and combination bands of complex mixtures, like film coatings, do not behave simply and cannot be directly interpreted. Variations in peak positions, changes in the area of each peak, and absorbance values of some bands are expected in the NIR spectra of polymer mixtures (Eldin, 2010). Therefore, it is impossible to resolve a useful reference for simple height or peak area quantitative methods. Band assignment of the individual excipients and PVA-based TiO_2 -free films presented in Table 2 is not always sufficient to make quantitative measurements and qualitative discriminations. Further quantitative and qualitative analysis will be performed using PCA/OPLS to extract the information from NIR spectral data (Roggo et al., 2007).

Table 2. Assignment of excipients' relevant overtones or combination bands

Wavenumber	PVA	PEG	Talc	Iron oxides	References
$10\,000\text{ cm}^{-1}$				${}^4\text{T}_{1g}$	(Scheinost and Schwertmann, 1997)
8319 cm^{-1}	O-H bending or stretching vibration				(Xie et al., 2016)
7185 cm^{-1}			$2\nu\text{Mg}_3\text{OH}$		(Petit et al., 2004)
7118 cm^{-1}			$2\nu\text{Mg}_2\text{FeOH}$		(Petit et al., 2004)
7156 cm^{-1}			$2\nu\text{Mg}_2\text{OH}$		(Petit et al., 2004)

7073 cm ⁻¹		2vFe ₂ OH	(Petit et al., 2004)
6925 cm ⁻¹	C-H bending vibration (could be influenced by PVA interaction with volatile compounds)		(Xie et al., 2016)
5834 cm ⁻¹	C=O stretching vibration		(Xie et al., 2016)
5761 cm ⁻¹		Second and third overtone of CH bend	(Snavelly et al., 1996)
5555 cm ⁻¹		CH stretch	(Snavelly et al., 1996)
5285 cm ⁻¹	O-H hydrogen bonding water exposed PVA OH		(Workman Jr. and Weyer, 2012)
5173 cm ⁻¹		OH bend	(Snavelly et al., 1996)
5150 cm ⁻¹	O-H interaction of multiple hydrogen atoms from poly(ethylene-co-vinyl alcohol) (EVOH) bonded to surrounding associated OH groups (from water) without clustering		(Workman Jr. and Weyer, 2012)
4812 cm ⁻¹	OH stretching OH bending		(Conzen et al., 2014)
4347.83 cm ⁻¹	C-H stretching C-H deformation		(Salah et al., 2020)
4324 cm ⁻¹		OH stretching	(Wu et al., 2022)
4331 cm ⁻¹		CH-stretching + CH-bending	(Wong et al., 1982)
4266 cm ⁻¹	C-H ₂ stretching + =C-H ₂ bending		(Conzen et al., 2014; Wong et al., 1982)
4180 cm ⁻¹		OH stretching	(Snavelly et al., 1996)
4054 cm ⁻¹			

3.3. Multivariate analysis

3.3.1. PCA analysis

PCA is a widely used unsupervised data analysis tool for large sets of highly co-linear data utilizing the entire wavenumber/wavelength range (Andersson et al., 2000; Jovanović et al., 2006). PCA was applied to explore the NIR dataset, identify spectral changes, and understand the most significant variance

sources. The analysis also aimed to locate systematic variation in the data matrix as the primary source of information on film growth. The model included 240 raw spectra (centered and scaled; no spectral filters applied) from different coating levels (coating suspension volumes: 3.6 L, 4.0 L, 4.3 L, 4.7 L). PCA was also used to relate the near-infrared spectra properties to the film properties and coating progression (Chang et al., 2001; Greenacre et al., 2022).

The PCA model was used for exploratory purposes without variable selection for the spectra, allowing us to better explain the spectral variations associated with the coating process and to identify the possible origins of the spectral features linked to the progress of film coating.

A PCA model of raw spectra showed that the spectral data could be accurately recovered as a linear combination of seven principal components (common spectral filters did not result in a smaller number of PCs). The percentage of explained variance and eigenvalues are presented in Table 3. The principal components were assessed for qualitative similarity to the change of interest, namely the progression of film coating determined by the peaks deemed important for film coating progression by domain knowledge (Tanabe et al., 2007). The first principal component (PC1) captures primary variance due to baseline absorbance or noise, indicated by its flat nature. Components 2 to 6 best represent the significant variances relevant to the PVA-based TiO₂-free film growth. The loadings are presented in Figure 6. Key spectral features identified include the band at 7185 cm⁻¹ (talc), prominent in PCs 3-6, and the 9696 cm⁻¹ band in PC5, likely influenced by the presence of iron oxide red and yellow. The band at 5141 cm⁻¹, especially prominent in PC3, corresponds to the decreasing signal of the tablet film and core, with a positive orientation of the PCA component loading due to PCA's arbitrary directionality. The band at 4324 cm⁻¹, which is absent in the core but present in the film, indicates the growth of film components and appears across multiple PCs. PC2 through PC6, particularly PC3 and PC5, effectively track the progression of the film coating.

The scatter plot (Figure S4) reveals distinct patterns with clearly separated clusters corresponding to different coating levels, along the principal components (PC3 and PC5). Coating levels 3.6L, 4.0L, and 4.3L cluster relatively close to each other along both PC3 and PC5, reflecting continuous coating progression and slight changes in their moisture content (confirmed by measured LOD values, Figure S5), which are expected during the constant spraying rate phase. 4.7L separates distinctly along both PC3 and PC5, representing the final coating level and moisture content which decreases further and to a greater extent during the drying phase (LOD values, Figure S5) (Möltgen et al., 2012). While, PC3 captures bulk moisture-related variance, from continuous spraying to drying (dominated by the 5141 cm⁻¹ peak), and general coating progression, in its loading PC5 contains features identified by domain knowledge as important for the film coating and a weaker contribution from the 5141 cm⁻¹ peak. This indicates that PC5 emphasizes coating-related features, while moisture plays a less significant role in the variance captured by this principal component. Although PC5 accounts for a smaller total amount of variance, it is important for explaining subtle changes during the film coating process. The coating level 4.7L behaves differently along PC5 compared to the other coating levels, reflecting the film coating characteristics as the drying phase concludes. A negligible number of outliers were identified in the scatter plot; however, their removal did not improve model performance.

Given that the principal component loadings capture the peaks identified through the knowledge-based approach, and that it was possible to visualize different clusters during the continuous spraying and

drying, it is considered appropriate to proceed with the development of predictive models for further analysis.

Table 3. PCA eigenvalues and percent variance explained by each PC

Principal component	Eigenvalues	% of variance	Cumulative variance
1	116.1	48.3	48.3
2	77.6	32.3	80.6
3	31.5	13.1	93.7
4	7.8	3.3	97.9
5	2.9	1.2	98.0
6	2.5	1.0	99.2
7	0.7	0.3	99.4

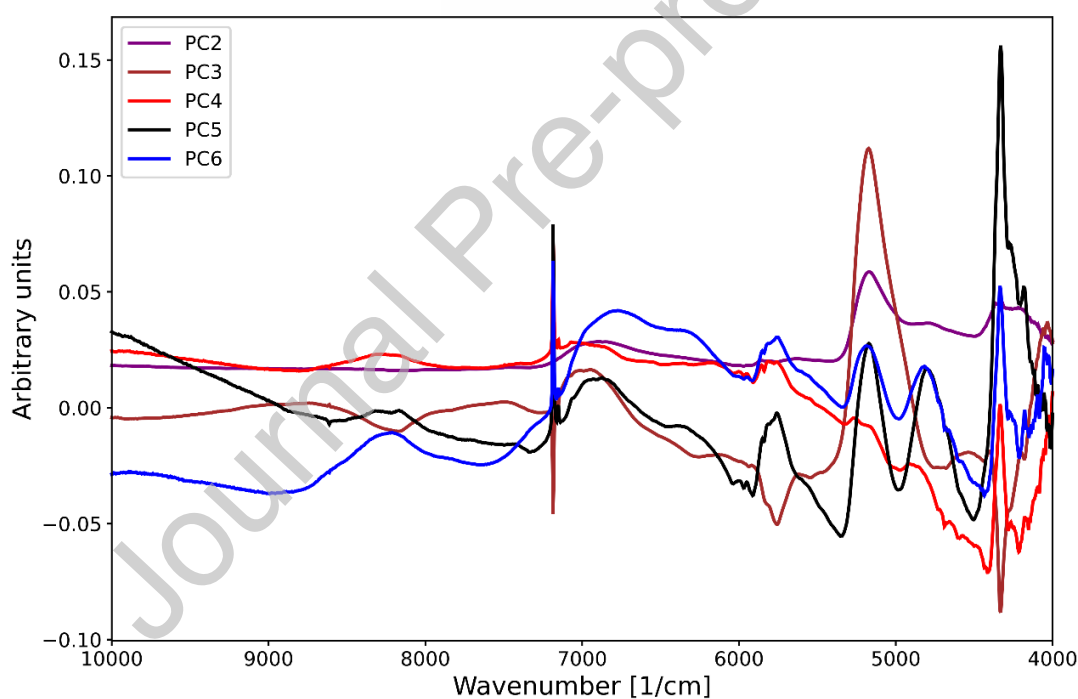


Figure 6. Loading plots for PCs 2 to 6 (PCs important for both film thickness and a^*) of the PCA model

These observations underscore the model's complexity and the importance of all six components in capturing the relevant spectral features. The PLS/OPLS methods are expected to be more robust and accurate than a correlation coefficient-based method using the PCs from PCA (PCA/MLR) concerning spectral variations as they focus only on important spectral variance for prediction and set spectral coefficients to low values for unimportant wavelengths. Hence, we will proceed using an OPLS model (Liu et al., 2022).

3.3.2. OPLS analysis

The rationale behind using OPLS in this analysis is that, unlike PLS, OPLS removes systematic variation in X that is orthogonal to Y and is expected to capture the relevant variation (film growth) in a predictive principal component. In contrast, the uncorrelated variation is fitted into orthogonal principal components. Concentrating the predictive information in one component increases the interpretability of the model (Eriksson et al., 2012).

An initial OPLS model was applied to raw, unprocessed spectra without variable selection to further understand the importance of the spectral signals for film thickness and a^* (CIELAB parameter). Results of quantitative analysis performed by applying OPLS analysis on raw spectra are presented in Table 4. Components were considered significant if their normalized eigenvalue exceeded 2 (Figure S8), which, in our case, led to the lowest RMSE_{cv}. Figure S9 illustrates this through the latent variable selection for the raw spectra model of film thickness.

Table 4. Results of OPLS calibration on raw and pre-processed spectra

Model calibration parameter	R ²	RMSEE	RMSE _{cv}	LV	RMSEP
Film thickness raw spectra	0.98	6.12 μm	6.23 μm	1+5+0	7.58 μm
a^* raw spectra	0.99	1.28	1.31	1+6+0	1.35
Film thickness pre-processed spectra ** (1 st -MSC)	0.95	5.00 μm	5.80 μm	1+6+0	7.00 μm
a^* pre-processed spectra ** (1 st -MSC)	0.99	0.90	0.92	1+6+0	1.20

** (1st-MSC)-1st derivative-Multiplicative Scatter Correction

The predictive component demonstrates the potential to separate different coating thickness levels for film thickness and a^* . The RMSE_{cv} and RMSEP are low, considering the maximum coating thickness of approximately 140 μm and maximum a^* of approximately 20, which is sufficient to discriminate between the sampled classes. The loading and coefficient plots for the calibration models for film thickness and a^* are presented in Figure 7 and Figure S6, respectively. There is an overall similarity in the coefficient trend for models calibrated with film thickness and a^* , which is expected considering they both increase as the film coating process progresses. The regression coefficients of the spectra, which represent the prediction vector for the selected Y, were further analyzed. The coefficient plots confirm that the most important wavelengths, which were determined by domain knowledge-based spectral analysis as well as PCA regression, namely 7185 cm^{-1} , 5141 cm^{-1} , and 4324 cm^{-1} , are also among the most important peaks for consideration in OPLS regression analysis and are representative of film growth as discussed previously. Additionally, the wavelengths from 10,000 cm^{-1} to 9000 cm^{-1} show a notably positive prediction vector for the film-coated tablets in that region. The score plots between the two calibration models are similar and will not be shown for brevity. The loading plots of film thickness and a^* resemble the PVA-based TiO₂-free film coating spectrum, indicating that all the relevant peaks from the domain knowledge analysis are used for film coating thickness prediction by the OPLS model. Figure 7a presents the overlaid loadings of

NIR calibration models with film thickness and a^* as reference methods. Figure 7b shows the overlaid spectra of the PVA-based TiO_2 -free film coating and the loading of the calibration model using film thickness as the reference method, demonstrating the importance of multiple peaks for calibration. Considering the reported OPLS regression model results on raw spectra, this model is effective to a certain extent at accommodating the impact of multiplicative scattering; however, further appropriate data pre-treatment may improve model performance and decrease complexity (Römer et al., 2008).

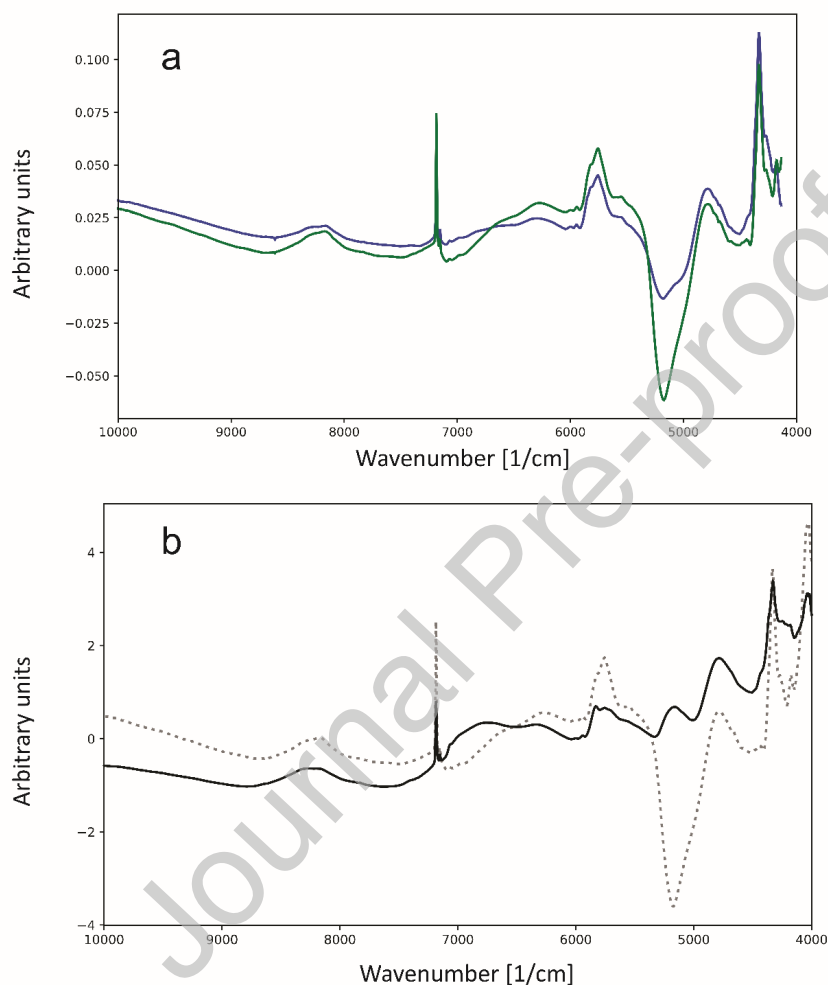


Figure 7. a) Overlaid loadings of NIR calibration models with film thickness (green line) and a^* (blue line) as reference methods (OPLS model; raw spectra) b) Overlaid plot of spectrum of PVA-based TiO_2 -free film coating and loading plot of the model with film thickness (dotted line -loading of calibration model with film thickness; full line -PVA-based TiO_2 -free film coating spectrum)

First derivative and MSC were applied to raw spectra to compensate for the light scattering effect and path length changes, improve quantification accuracy, remove the baseline shift, and enhance spectral resolution. First derivative, followed by MSC, made the variance more obvious and distinctly separated the coating levels based on the previously determined relevant wavelengths. Furthermore, distinct

regions of the spectra at different coating levels are more apparent in the preprocessed spectra than in the raw spectra (Figures S7a and S7b - raw spectra; Figures S7c and S7d - preprocessed spectra with first derivative and MSC). The statistical indicators of the model are presented in Table 4. The results demonstrate that the differences among the model prediction capabilities are negligible when the data is preprocessed using the first derivative and MSC. Figure 8 presents the measured versus predicted plots for film thickness and a^* for both the training and test sets. The robustness of the model for film thickness and a^* prediction is further confirmed by DModY and normalized N-residual plots of the test set (Figures S10–S13). The DModY plots illustrate the normalized prediction error across different observations. There are no outliers or clear trends for film thickness or a^* , where the model either over or under-predicts. The residuals are approximately normally distributed, and there are no notable positive or negative deviations or outliers, suggesting a robust model. The literature reports a maximum NIR penetration depth of 300 μm in TiO_2 films, enabling simultaneous data acquisition from both the core and coating, which is essential for robust model development. However, no such data exist for TiO_2 -free films. Our studies indicate that the model accurately predicts without significant under- or overestimation regardless of the coating thickness and process progression (Möltgen et al., 2012; Römer et al., 2008). These models will be tested and repeatedly used in practical settings to further evaluate the effect of baseline removal on predictive ability. This will help in choosing the most robust model with satisfactory accuracy. The relationship between film coating thickness and changes in color parameters in the pharmaceutical industry has not been fully explored. The use of a color parameter as a reference technique should be based on a clear understanding of the relationship between film thickness and color changes. With proper justification, this approach offers a non-invasive method for calibration or re-calibration, making it potentially appropriate as a reference technique in NIR applications. In addition, the capability of NIR spectroscopy in the presence of various TiO_2 substitutes as opacifiers has not been fully explored. Future studies should investigate a broader range of film coating materials and thicknesses to better understand the potential of using CIELAB as a reference technique for colored films. Through further research, valuable insights could be gained for developing in-line models and novel calibration methods, potentially improving process understanding.

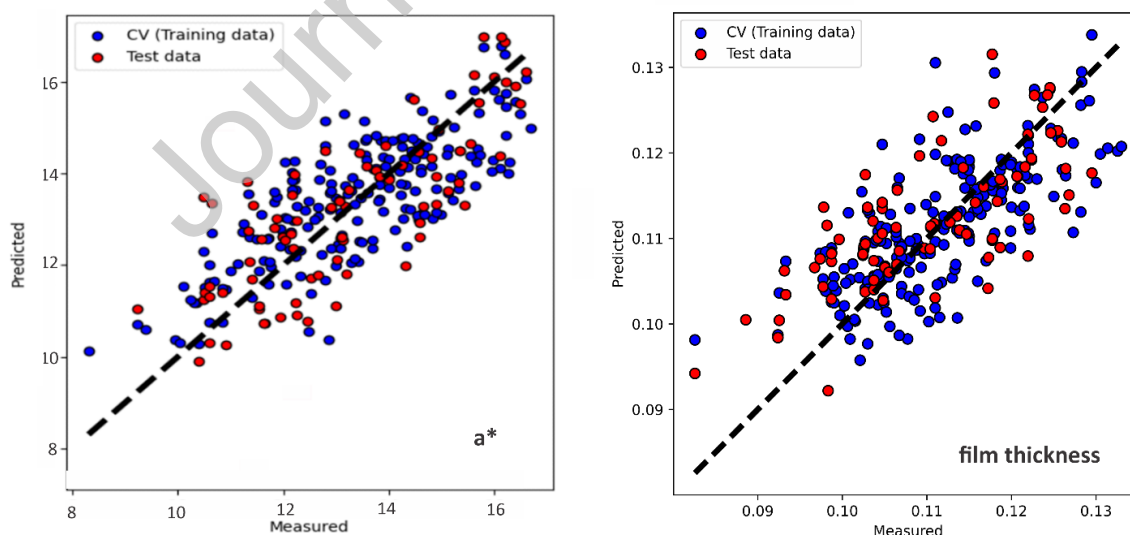


Figure 8. Measured vs predicted for models with a^* and film thickness as reference methods (1st derivative and MSC models)- training and test set

4. Conclusion

This study demonstrates that FT-NIR spectroscopy is a highly sensitive and effective tool for off-line monitoring of TiO₂-free film coating processes. By utilizing film thickness measurements and the a* parameter from the CIELAB color space as reference methods, changes during the coating progression were effectively described and predicted. PCA revealed spectral features associated with the progression of film coating, illustrated through variations across multiple principal components. Domain knowledge spectral analysis identified several bands of interest, which were confirmed via OPLS analysis of loading and coefficient plots. OPLS analysis on preprocessed spectra using the first derivative and MSC resulted in low prediction errors for both film thickness (RMSE_{cv} = 5.80 μm; RMSEP = 7.00 μm) and the a* parameter (RMSE_{cv} = 0.92; RMSEP = 1.20), indicating the robustness of the models. These findings indicate that FT-NIR spectroscopy, combined with multivariate analysis, can be employed as a rapid and robust method for predicting tablet coating quality parameters based on objective measurements of chemical signals from all film components.

CRedit authorship contribution statement

Filip Gorachinov: Methodology, Investigation, Data analysis, Data visualization, Writing – original draft, review & editing. **Monika Koviloska:** Investigation, Data analysis, Writing – review & editing. **Katerina Tnokovska:** Conceptualization, Methodology, Investigation, Data analysis, Writing – original draft, review & editing. **Ana Atanasova:** Conceptualization, Methodology, Writing – review & editing, Supervision. **Packa Antovska:** Conceptualization, Methodology, Writing – original draft, review & editing. **Jelena Lazova:** Conceptualization, Methodology, Writing – review & editing, Supervision. **Nikola Geskovski:** Conceptualization, Methodology, Investigation, Data analysis, Writing – original draft, review & editing, Supervision.

Declaration of competing interest

The authors have no conflicts of interest to disclose.

Data availability

Data will be made available on request.

References

- Alves-Lima, D., Song, J., Li, X., Portieri, A., Shen, Y., Zeitler, J.A., Lin, H., 2020. Review of Terahertz Pulsed Imaging for Pharmaceutical Film Coating Analysis. *Sensors (Basel)* 20, 1441. <https://doi.org/10.3390/S20051441>
- Andersson, M., Folestad, S., Gottfries, J., Johansson, M.O., Joseffson, M., Wahlund, K.G., 2000. Quantitative analysis of film coating in a fluidized bed process by in-line NIR spectrometry and multivariate batch calibration. *Anal. Chem.*, 72, 2099–2108. <https://doi.org/10.1021/AC990256R>
- Beć, K.B., Grabska, J., Huck, C.W., 2020. Near-Infrared Spectroscopy in Bio-Applications. *Molecules.*, 25, 2948. <https://doi.org/10.3390/MOLECULES25122948>

- Ben-Dor, E., 2002. Quantitative remote sensing of soil properties. *Adv. Agron.*, 75, 173–243.
[https://doi.org/10.1016/S0065-2113\(02\)75005-0](https://doi.org/10.1016/S0065-2113(02)75005-0)
- Blundell, R., Butterworth, P., Charlier, A., Daurio, D., Degenhardt, M., Harris, D., Hancock, B., Johnston, M., Kasina, R., Kaye, J., Kelly, R., Lienbacher, P., Meehan, L., Melnick, J., Ojakovo, P., Schoell, J., Schimmelle, B., Tobyn, M., Wagner-Hattler, L., Wakeman, J., Wiedey, R., 2022. The Role of Titanium Dioxide (E171) and the Requirements for Replacement Materials in Oral Solid Dosage Forms: An IQ Consortium Working Group Review., *J. Pharm. Sci.*, 111, 2943–2954.
<https://doi.org/10.1016/J.XPHS.2022.08.011>
- Brock, D., Zeitler, J.A., Funke, A., Knop, K., Kleinebudde, P., 2012. A comparison of quality control methods for active coating processes. *Int. J. Pharm.*, 15;439(1-2):289-95. doi: 10.1016/j.ijpharm.2012.09.021
- Chen C.P.J., White, R., 2024. Common Pitfalls in Evaluating Model Performance and Strategies for Avoidance. SSRN. <https://dx.doi.org/10.2139/ssrn.4829509>
- Ciurczak, E.W., Igne, B., Workman, J. Jr., Burns, D.A., 2021. *Handbook of Near infrared spectroscopy*, 4th Ed., CRC Press, Boca Raton.
- Conzen, J. P., 2014. *Multivariate Calibration, A Practical Guide for Developing Methods in the Quantitative Analytical Chemistry*, Bruker Optik GmbH, Ettlingen, Germany
- Czajkowska, M., Sznitowska, M., Kleinebudde, P., 2015. Determination of coating thickness of minitables and pellets by dynamic image analysis., *Int. J. Pharm.*, 495, 347–353.
<https://doi.org/10.1016/J.IJPHARM.2015.08.102>
- Snavely, D. L., Dubsky, J., 1996. Near-IR spectra of polyethylene, polyethylene glycol, and polyvinylethyl ether., *J. Polym. Sci. A, Polym. Chem.*, 34 (13), 2575-2579. [https://doi.org/10.1002/\(SICI\)1099-0518\(19960930\)34:13<2575::AID-POLA3>3.0.CO;2-R](https://doi.org/10.1002/(SICI)1099-0518(19960930)34:13<2575::AID-POLA3>3.0.CO;2-R)
- Dong, R., Nassar, M., Friend, B., Teckoe, J., Zeitler, J., 2023. Studying the dissolution of immediate release film coating using terahertz pulsed imaging. *Int. J. Pharm.*, 630, 122456.
<https://doi.org/10.1016/J.IJPHARM.2022.122456>
- Eldin, A.B., 2010. *Near Infra-Red Spectroscopy. Wide Spectra of Quality Control*. InTech; 2011.
<http://dx.doi.org/10.5772/24208>
- Eriksson, L., Rosén, J., Johansson, E., Trygg, J., 2012. Orthogonal PLS (OPLS) Modeling for Improved Analysis and Interpretation in Drug Design. *Mol. Inform.*, 31, 414–419.
<https://doi.org/10.1002/MINF.201200158>
- European Medicines Agency, 2014. *Guideline on the use of Near Infrared Spectroscopy (NIRS) by the pharmaceutical industry and the data requirements for new submissions and variations*.
- Farkas, D., Madarász, L., Nagy, Z.K., Antal, I., Kállai-Szabó, N., 2021. Image Analysis: A Versatile Tool in the Manufacturing and Quality Control of Pharmaceutical Dosage Forms. *Pharmaceutics*, 13, 685.
<https://doi.org/10.3390/PHARMACEUTICS13050685>

- Ficzere, M., Mészáros, L.A., Kállai-Szabó, N., Kovács, A., Antal, I., Nagy, Z.K., Galata, D.L., 2022. Real-time coating thickness measurement and defect recognition of film coated tablets with machine vision and deep learning. *Int. J. Pharm.*, 623, 121957. <https://doi.org/10.1016/j.ijpharm.2022.121957>
- Gallo, N.D., Elia, A-G., Knuettel, A.N., Riedel, M., von der Brelie, A., Kipping, T., 2023. Calcium carbonate as a replacement for titanium dioxide in coating: the importance of particle engineering, SAFC, Lit. No. MK_PS12784EN.
- Gendre, C., Genty, M., Boiret, M., Julien, M., Meunier, L., Lecoq, O., Baron, M., Chaminade, P., Péan, J.M., 2011. Development of a Process Analytical Technology (PAT) for in-line monitoring of film thickness and mass of coating materials during a pan coating operation. *Eur. J. Pharm. Sci.*, 43, 244–250. <https://doi.org/10.1016/J.EJPS.2011.04.017>
- Haaser, M., Gordon, K.C., Strachan, C.J., Rades, T., 2013. Terahertz pulsed imaging as an advanced characterisation tool for film coatings - A review. *Int. J. Pharm.*, 457, 510–520. <https://doi.org/10.1016/J.IJPHARM.2013.03.053>
- Hattori, Y., Sugata, M., Kamata, H., Nagata, M., Nagato, T., Hasegawa, K., Otsuka, M., 2018. Real-time monitoring of the tablet-coating process by near-infrared spectroscopy - Effects of coating polymer concentrations on pharmaceutical properties of tablets. *J. Drug. Deliv. Sci. Technol.*, 46, 111–121. <https://doi.org/10.1016/J.JDDST.2018.04.018>
- Xie, J.C., Yuan, H.F., Yan, X.J., Zhao, X.L., Song, C.F., Wang, X.M., Li, X.Y., 2016. [Determination of Alcoholysis Degree and Volatile Matter of Poly-Vinyl Alcohol Using Diffuse-Reflection Near Infrared Spectroscopy] - *Guang Pu Xue Yu Guang Pu Fen Xi.*, 36(1):70-4. [https://doi.org/10.3964/j.issn.1000-0593\(2016\)01-0070-05](https://doi.org/10.3964/j.issn.1000-0593(2016)01-0070-05)
- Jovanović, N., Gerich, A., Bouchard, A., Jiskoot, W., 2006. Near-infrared imaging for studying homogeneity of protein-sugar mixtures. *Pharm. Res.*, 23, 2002–2013. <https://doi.org/10.1007/S11095-006-9037-Y>
- Li, C., Zeitler, J.A., Dong, Y., Shen, Y.C., 2014. Non-destructive evaluation of polymer coating structures on pharmaceutical pellets using full-field optical coherence tomography. *J. Pharm. Sci.*, 103, 161–166. <https://doi.org/10.1002/JPS.23764>
- Liu, C., Zhang, X., Nguyen, T.T., Liu, J., Wu, T., Lee, E., Tu, X.M., 2022. Partial least squares regression and principal component analysis: similarity and differences between two popular variable reduction approaches. *Gen. Psychiatr.*, 35, e100662. <https://doi.org/10.1136/GPSYCH-2021-100662>
- Markl, D., Hanneschläger, G., Sacher, S., Leitner, M., Buchsbaum, A., Pescod, R., Baele, T., Khinast, J.G., 2015. In-Line Monitoring of a Pharmaceutical Pan Coating Process by Optical Coherence Tomography. *J. Pharm. Sci.*, 104, 2531–2540. <https://doi.org/10.1002/JPS.24531>
- Maurer, L., Leuenberger, H., 2009. Terahertz pulsed imaging and near infrared imaging to monitor the coating process of pharmaceutical tablets. *Int. J. Pharm.*, 370, 8–16. <https://doi.org/10.1016/J.IJPHARM.2008.11.011>

- Möltgen, C. V., Puchert, T., Menezes, J.C., Lochmann, D., Reich, G., 2012. A novel in-line NIR spectroscopy application for the monitoring of tablet film coating in an industrial scale process. *Talanta*, 92, 26–37. <https://doi.org/10.1016/J.TALANTA.2011.12.034>
- Morris, R. V., Lauer, H. V., Lawson, C.A., Gibson, E.K., Nace, G.A., Stewart, C., 1985. Spectral and other physicochemical properties of submicron powders of hematite (α -Fe₂O₃), maghemite (γ -Fe₂O₃), magnetite (Fe₃O₄), goethite (α -FeOOH), and lepidocrocite (γ -FeOOH). *J. Geophys. Res.*, 90, 3126–3144. <https://doi.org/10.1029/JB090IB04P03126>
- Mortimer, R.J., Graham, K.R., Grenier, C.R.G., Reynolds, J.R., 2009. Influence of the Film Thickness and Morphology on the Colorimetric Properties of Spray-Coated Electrochromic Disubstituted 3,4-Propylenedioxythiophene Polymers. *ACS Appl. Mater. Interfaces*, 1, 2269–2276. <https://doi.org/10.1021/am900431z>
- Mostafaei, F., Khinast, J.G., Remmelgas, J., Forgber, T., 2023. Simultaneous optimization of inter- and intra-tablet coating variability in a lab-scale coating process via DEM-MC simulations. *Powder Technol.*, 428, 118788. <https://doi.org/10.1016/J.POWTEC.2023.118788>
- Murillo, M.A., Rodríguez-Pulido, F.J., Heredia, F.J., Melgosa, M., Pacheco, J., Vargas, R., Montero, E., Gutiérrez, D., 2018. Color evolution during a coating process of pharmaceutical tablet cores by random spraying. *Color. Res. Appl.*, 44, 1–8. <https://doi.org/10.1002/COL.22332>
- Palugan, L., Spoldi, M., Rizzuto, F., Guerra, N., Uboldi, M., Cerea, M., Moutaharrik, Saliha Melocchi, Alice Gazzaniga, Andrea, Zema, L., 2022. What's next in the use of opacifiers for cosmetic coatings of solid dosage forms? Insights on current titanium dioxide alternatives. *Int. J. Pharm.*, 25, 121550. <https://doi.org/doi:10.1016/j.ijpharm.2022.121550>
- Petit, S., Martin, F., Wiewiora, A., De Parseval, P., Decarreau, A., 2004. Crystal-chemistry of talc: A near infrared (NIR) spectroscopy study. *American Mineralogist*, 89, 319–326. <https://doi.org/10.2138/AM-2004-2-310>
- Pomerantsev, A.L., Rodionova, O.Y., Skvortsov, A.N., 2017. Diffuse Reflectance Spectroscopy of Hidden Objects, Part I: Interpretation of the Reflection–Absorption–Scattering Fractions in Near-Infrared (NIR) Spectra of Polyethylene Films. *Appl. Spectrosc.*, 71, 1760–1772. <https://doi.org/10.1177/0003702817694182>
- Radtke, J., Wiedey, R., Kleinebudde, P., 2021. Alternatives to titanium dioxide in tablet coating. *Pharm. Dev. Technol.*, 26, 989–999. <https://doi.org/10.1080/10837450.2021.1968900>
- Roggo, Y., Chalus, P., Maurer, L., Lema-Martinez, C., Edmond, A., Jent, N., 2007. A review of near infrared spectroscopy and chemometrics in pharmaceutical technologies. *J. Pharm. Biomed. Anal.*, 44, 683–700. <https://doi.org/10.1016/J.JPBA.2007.03.023>
- Römer, M., Heinämäki, J., Strachan, C., Sandler, N., Yliruusi, J., 2008. Prediction of tablet film-coating thickness using a rotating plate coating system and NIR spectroscopy. *AAPS Pharm. Sci. Tech.*, 9, 1047–1053. <https://doi.org/10.1208/S12249-008-9142-9>

- Salah, M., Gad, M., Elkattan, M., Sabry, Y., 2020. Optical constants of gamma-irradiated silver-doped PVA in the near-infrared range. *Micro Nano Lett.*, 15, 480–485.
<https://doi.org/10.1049/MNL.2019.0800>
- Scheinost, A.C., Schwertmann, U., 1997. VIS-NIR reflectance spectra of goethite (alpha-Fe-OOH) as a function of particle size, unit cell size, and cation substitution. *Lunar and Planetary Science*, 1243.
- Schindelin, J., Arganda-Carreras, I., Frise, E., Kaynig, V., Longair, M., Pietzsch, T., Preibisch, S., Rueden, C., Saalfeld, S., Schmid, B., Tinevez, J.Y., White, D.J., Hartenstein, V., Eliceiri, K., Tomancak, P., Cardona, A., 2012. Fiji: an open-source platform for biological-image analysis. *Nature Methods*, 9:7 9, 676–682. <https://doi.org/10.1038/nmeth.2019>
- Tanabe, H., Otsuka, K., Otsuka, M., 2007. Theoretical analysis of tablet hardness prediction using chemoinformetric near-infrared spectroscopy. *Anal. Sci.*, 23, 857–862.
<https://doi.org/10.2116/ANALSCI.23.857>
- Turk, M., Šibanc, R., Dreu, R., Frankiewicz, M., Sznitowska, M., 2021. Assessment of Mini-Tablets Coating Uniformity as a Function of Fluid Bed Coater Inlet Conditions. *Pharmaceutics*, 13, 746.
<https://doi.org/10.3390/PHARMACEUTICS13050746>
- Wahl, P.R., Peter, A., Wolfgang, M., Khinast, J.G., 2019. How to measure coating thickness of tablets: Method comparison of optical coherence tomography, near-infrared spectroscopy and weight-, height- and diameter gain. *Eur. J. Pharm. Biopharm.*, 142, 344–352.
<https://doi.org/10.1016/J.EJPB.2019.06.021>
- Wolfgang, M., Peter, A., Wahl, P., Markl, D., Zeitler, J.A., Khinast, J.G., 2019. At-line validation of optical coherence tomography as in-line/at-line coating thickness measurement method. *Int. J. Pharm.*, 572, 118766. <https://doi.org/10.1016/J.IJPHARM.2019.118766>
- Wong, J.S., MacPhall, R.A., Moore, C.B., Strauss, H.L., 1982. Local mode spectra of inequivalent C-H oscillators in cycloalkanes and cycloalkenes. *J. Phys. Chem.*, 86, 1478–1484.
<https://doi.org/10.1021/J100397A054>
- Workman J.Jr., Weyer, L., 2012. *Practical Guide and Spectral Atlas for Interpretive Near-Infrared Spectroscopy*, CRC Press. <https://doi.org/10.1201/b11894>
- Wu, H., He, M., Wu, S., Yang, M., Liu, X., 2022. Near-Infrared Spectroscopy Study of OH Stretching Modes in Pyrophyllite and Talc. *Crystals (Basel)* 12, 1759. <https://doi.org/10.3390/CRYST12121759>
- Zaid, A.N., 2020. A Comprehensive Review on Pharmaceutical Film Coating: Past, Present, and Future. *Drug. Des. Devel. Ther.*, 14, 4613-4623. <https://doi.org/10.2147/DDDT.S277439>
- Zhang, Q., Wan, H., Hu, G., 2018. Comparisons of Inter-tablet Coating Variability under Different Tablet Shapes and Filling Levels by Using DEM Simulations. *MATEC Web of Conferences*, 238 (04008).
<https://doi.org/10.1051/matecconf/201823804008>
- Zheng, G., Ryu, D., Jiao, C., Xie, X., Cui, X., Shang, G., 2019. Visible and near-infrared reflectance spectroscopy analysis of a coastal soil chronosequence. *Remote. Sens. (Basel)*, 11, 2336.
<https://doi.org/10.3390/RS11202336>

Graphical abstract

